Acta Cryst. (1998). B**54**, 384–390

Prediction of Early- and Late-Growth Morphologies of Ionic Crystals

L. J. Soltzberg,* Olinda Carneiro, Gillianne S. Joseph, Zahida Khan, Tami D. Meretsky, Mai Mai Ng and Sharon A. Ofek

Department of Chemistry, Simmons College, 300 The Fenway, Boston, MA 02115, USA.
E-mail: lsoltzberg@vmsvax.simmons.edu

(*Received 9 October 1997; accepted 11 February 1998*)

Abstract

Comparison of early- and late-growth crystal morphologies of several water-soluble ionic materials suggests that early rapid growth is accompanied by a specific type of morphological distortion. This distortion, involving a change in the *relative* growth rate of just one growth direction, is consistent with our previously proposed mechanism for the transition from normal, polyhedral crystal growth to dendritic growth. Interpretation of this morphological distortion was aided by morphology prediction methods based on computed attachment energies.

1. Introduction

The relationship of dendritic (treelike) crystal morphology to normal growth morphology has been a subject of interest, in part because of the implications of crystal morphology for the physical properties of materials and for process engineering (Green *et al.*, 1996). We have been studying the growth of dendritic crystals in order to understand the relationship between the dendritic and normal morphologies of specific substances, and in order to elucidate the nature of the transition from normal growth to dendritic growth which occurs when growth rate is increased (Soltzberg *et al.*, 1992; Soltzberg *et al.*, 1994).

Work to-date has suggested that the transition to dendritic morphology has its basis in the different growth mechanisms that prevail at different crystal faces. Crystal morphology is affected by the competition between growth at emergent screw dislocations *versus* growth by two-dimensional nucleation of new kinks on existing crystal faces (Lewis, 1974*a*,*b*). Measurements on the morphological distortions which occur at the transition from normal polyhedral crystal growth to dendritic growth indicate that, at a critical growth rate, certain growth directions begin to add material at a disproportionately high rate. This distortion causes protrusions from the corners of the normal crystal to reach out toward regions of high solute concentration (in the case of growth from solution) or of low temperature, in the case of growth from the melt (Chan *et al.*, 1976); there is, thus, a positive feedback between morphological distortion of the crystal and the driving force for crystal growth itself (supersaturation or supercooling). This combination of factors leads to the branching coherent aggregate of crystalline needles that is termed a dendrite (Soltzberg *et al.*, 1994).

The question naturally arises as to what is special about the crystal growth directions that become the dendrite branches. Qualitatively, we have suggested that the slow-growing directions corresponding to the faces of the normal crystal are those that grow by the screw dislocation mechanism (Burton *et al.*, 1951). Such faces have a different relationship of growth rate to supersaturation than faces which grow by two-dimensional nucleation (Kuroda *et al.*, 1987; Lewis, 1974*a*). Since the transition from normal to dendritic habit can be considered to be an extreme case of crystal habit modification, we have attempted to apply more quantitative methods of morphology prediction to see what light could be shed on the dendritic morphology.

The various approaches to crystal morphology prediction have been summarized by Docherty *et al.* (1991). Considerable success in predicting the morphologies of molecular crystals has been achieved through the use of the 'attachment energy' method. Here, the growing crystal is considered to consist of the bulk crystal (that which has already grown) and a crystal slice of a certain orientation (*hkl*) and thickness (d_{hkl}) about to attach to the bulk. The energy of the bulk is computed by summing atom–atom potentials over a sufficiently large volume to achieve convergence. The slice energy is similarly computed and the attachment energy is taken as the difference between the bulk energy and the slice energy; that is, the bulk energy per mole of crystal is the sum of the slice energy and the attachment energy. The attachment energy can be computed for any crystal direction. Directions corresponding to high attachment energies are assumed to grow rapidly and thus do not appear as faces in the mature crystal, while those directions with low attachment energies become the faces of the crystal.

Application of this method to ionic crystals is computationally more difficult than for molecular crystals, because the long-range Coulomb forces require a much larger summation sphere in order to achieve convergence (Karasawa & Goddard III, 1989). Recently

developed software (Gay & Rohl, 1995) incorporates a method suggested by Ewald (1921, long before the advent of digital computers!) in computing the slice and bulk energies; these two- and three-dimensional Ewald sums, which divide the summation into real-space and reciprocal-space components, greatly reduce the computational cost of determining attachment energies for ionic crystals.

The attachment energy method has been applied to several ionic crystals in recent years (Gay & Rohl, 1995; Hartman & Strom, 1989; Roberts *et al.*, 1995). These studies have taken into account not only the Coulombic attractive forces in such crystals, but also short-range attractive and repulsive forces. The method, which has been described in detail by Telfer *et al.* (1996), involves refining an initial set of X-ray or neutron diffraction atomic coordinates plus the parameters of the various potentials against a group of experimental data, including elastic constants, dielectric constants and phonon frequencies. The structure and potentials thus obtained (the 'refined structure') are then used for the computation of attachment energies. In the present work we have dispensed with the short-range potentials and thus with the refinement process, and have used only the Coulomb attractions computed from published X-ray or neutron diffraction atomic coordinates. This approach has given satisfactory results in the cases studied, presumably because Coulomb interactions so dominate the lattice energy in the ionic compounds chosen.

2. Experimental

In the present work we studied crystals of six different water-soluble ionic materials: KNO_3, $RbNO_3$, $KClO_4$, NH_4NO_3 (IV), NH_4NO_3 (III) and $KClO_3$. Crystals were grown by controlled cooling from solutions saturated at various starting temperatures. In the case of NH_4NO_3 (III) we employed the method of Choi & Prask (1982), in which the high-temperature polymorph is stabilized at room temperature by the addition of 5% by weight KNO_3. The apparatus and method for growing crystals have been detailed previously (Soltzberg *et al.*, 1994). In the present work we grew crystals both in chamber slides and in small covered beakers. Crystals were grown at initial dimensionless supercoolings† as follows: KNO_3 (0.03), $RbNO_3$ (0.07), $KClO_4$, (0.02), NH_4NO_3 (IV) (0.01), NH_4NO_3 (III) (0.03) and $KClO_3$ (0.01). Crystal growth was recorded using a microscope-mounted video camera and a time-lapse VCR.

† Dimensionless supercooling is $\Delta = (C_\infty - C_{eq})/(C_s - C_{eq})$, where C_∞ is the concentration of the high-temperature saturated solution before cooling, C_{eq} is the equilibrium concentration of the solution at the low temperature at which the crystal is growing and C_s is the 'concentration' of the solid (Dougherty *et al.*, 1987.

Table 1. *Coulomb-only lattice energies*

	Space group	$E_{lattice}$ (this work), eV mol^{-1}	$E_{lattice}$ (literature), eV mol^{-1}	% difference
KNO_3	*Pnma*	7.27	7.12	2.1
$KClO_4$	*Pnma*	6.48	6.24	3.8
$RbNO_3$	$P3_1$	6.57	6.82	3.7
NH_4NO_3 (IV)	*Pmmn*	7.02	7.01	0.1
NH_4NO_3 (III)	*Pnma*	7.00	—	—
$KClO_3$	$P2_1/m$	7.35	7.32	0.4

Morphologies of the resulting crystals were determined using X-ray precession photographs to determine orientation and optical goniometry to determine the identities of the crystal faces.

The transition from normal to dendritic growth in $RbNO_3$ was studied using double-beam interference microscopy, as described elsewhere (Soltzberg *et al.*, 1994).

3. Computations

Lattice energies and attachment energies were computed using *MARVIN* (Gay & Rohl, 1995). The unit-cell parameters and atomic coordinates needed for these *MARVIN* computations were taken from the literature: KNO_3 (Nimmo & Lucas, 1973), $RbNO_3$ (Dean *et al.*, 1984), $KClO_4$ (Johansson & Lindqvist, 1977), NH_4NO_3 (IV) (Choi *et al.*, 1972), NH_4NO_3 (III) (Choi & Prask, 1982) and $KClO_3$ (Bats, 1978). In the case of the disordered NH_4NO_3 (III) structure we used the coordinates for one of the two sets of H-atom positions. We did not employ relaxation of the surfaces, as is often performed with *MARVIN* computations (Rohl & Gay, 1996); such relaxation would necessarily fail with our Coulomb-only potential.

It has been shown that the values used for atomic charges, especially those within a polyatomic ion, can significantly affect predicted crystal morphologies (Hartman & Strom, 1989). We employed *MacSPARTAN Plus* (Wavefunction Inc., 1997) for *ab initio* computations at the 6-31G* level of theory for isolated NO_3^-, ClO_4^- and ClO_3^- ions; atomic charges were fit to the resulting electrostatic potential. The NH_4NO_3 polymorphs involve hydrogen bonding, which might be expected to affect the charge distributions within the NH_4^+ and NO_3^- ions. Here, we used the charges computed for the cluster $(NH_4NO_3NH_4)^+$. However, no special potentials were used to describe the hydrogen bonding in the lattice energy and attachment energy computations for the NH_4NO_3 polymorphs.

Crystal morphologies were visualized using *SHAPE* (Dowty & Richards, 1993). The use of this program for morphology prediction is based on the Wulff theorem that the faces bounding a crystal are those with small surface energies (Brice, 1973), except that we used attachment energies rather than surface energies

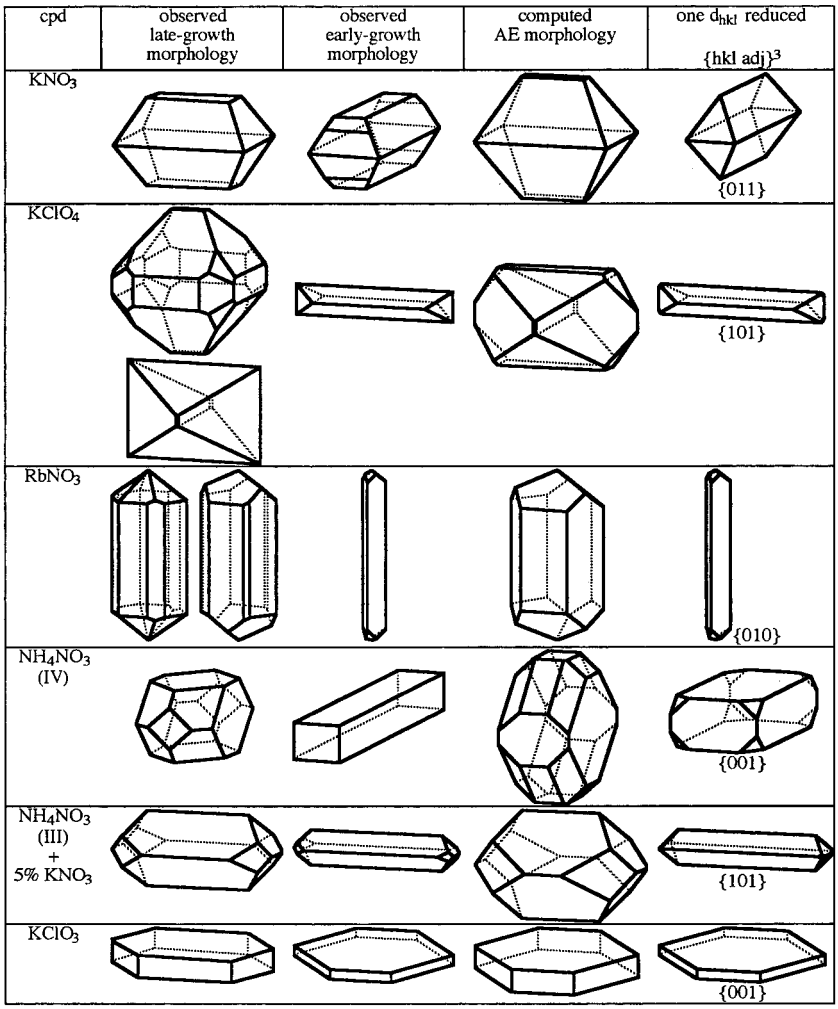

Fig. 1. Observed and predicted morphologies. All renderings have the standard clinographic orientation, with the *a* axis emerging from the page, the *b* axis roughly horizontal, but tilted slightly from the page, and the *c* axis nearly vertical, but tilted very slightly out of the page. *hkl* is the direction that has been adjusted to duplicate the early-growth morphology.

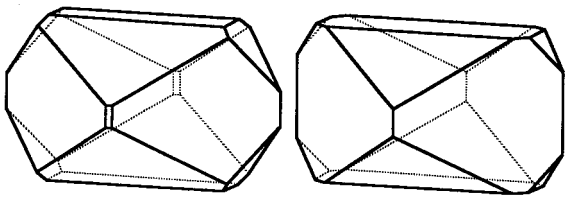

(*a*) (*b*)

Fig. 2. (*a*) $KClO_4$ morphology predicted from attachment energies computed with Coulomb-only interactions (this work). (*b*) $KClO_4$ morphology from attachment energies including short-range interactions (Roberts *et al.*, 1995).

(Bennema *et al.*, 1993). The unit-cell dimensions, the list of Miller indices for low-index faces and the corresponding attachment energies from *MARVIN* (Gay & Rohl, 1995) are used as input into *SHAPE* (Dowty & Richards, 1993). In general, the smaller the attachment energy the more prominent a face will be, although the specific geometry of the crystal affects just how small an attachment energy must be for a face to appear in the predicted morphology. To depict the crystals observed in the laboratory, we manipulated the *SHAPE* (Dowty & Richards, 1993) input to duplicate the observed gross† and detailed morphologies.

Crystal structures and surfaces at the molecular level were visualized using the program *CrystalDesigner* (Crystal Structure Design, AS, 1997).

4. Results and discussion

The observed crystal morphologies are summarized in the first two columns of drawings in Fig. 1. Each of the renderings in these two columns corresponds to videotape frames of actual crystals. Comparison of column 3 with column 1 (Fig. 1) shows excellent agreement between morphologies predicted from the attachment energies and the observed late-growth morphologies.

† We distinguish between the gross morphology of a crystal, *i.e.* elongated, tabular or equant, and the detailed morphology, referring to which faces are present.

The predictions of both gross morphology and detailed morphology agree well with the observed morphologies shown in column 1. The successful prediction of morphology with Coulomb-only attachment energies indicates, not surprisingly, that electrostatic forces dominate the energy balance in these ionic crystals; this conclusion is borne out by agreement between the Coulomb-only lattice energies computed by *MARVIN* and literature values based on thermochemical data, summarized in Table 1, and by the very small effect of including short-range interactions, shown in Fig. 2. It must be appreciated, however, that the prediction of crystal properties beyond morphology would require the inclusion of the short-range potentials.

For the materials we have studied so far there appears to be a systematic difference in the gross morphology of the 'mature' crystals (crystals grown slowly or maintained at equilibrium with the mother liquor for an extended period following initial growth) and early-growth crystals (grown more rapidly, but not so rapidly as to form dendrites). In KNO_3, $RbNO_3$, NH_4NO_3 (IV), NH_4NO_3 (III) and $KClO_4$ the morphology distortion in the early-growth crystals takes the form of pronounced elongation in one direction. In $KClO_3$ the distortion is a pronounced flattening. In each case the more rapidly grown crystal shows a distortion of morphology corresponding to one direction growing more slowly, relative to all other directions, than in the mature crystal.

It is of special interest that we can simulate the morphological distortions recorded in column 2 by starting from the attachment energy morphologies (column 3) and, in each case, artificially reducing the attachment energy for just one growth direction. The resulting morphologies are shown in column 4. Reduction of an attachment energy in this manner corresponds physically either to a reduction in the growth rate in this direction relative to all other directions, or, alternatively, to an increase in the growth rate of all directions relative to this one. It is the latter interpretation that offers an explanation for the distortions observed in early-growth crystals.

Crystal surfaces with low Miller indices add new material at emergent screw dislocations or by two-dimensional nucleation of new growth centers on existing planes (Lewis, 1974*a*; Sunagawa, 1981, 1987). For very low Miller-index planes, the kinetics are more favorable for addition at dislocations. The rate of growth by both mechanisms has been studied in detail; under the conditions that prevail for crystal growth from solution or from the melt, for a face that can grow by both mechanisms, the growth rate at dislocations will typically be faster at low supersaturation, while above a critical supersaturation the rate of growth by nucleation

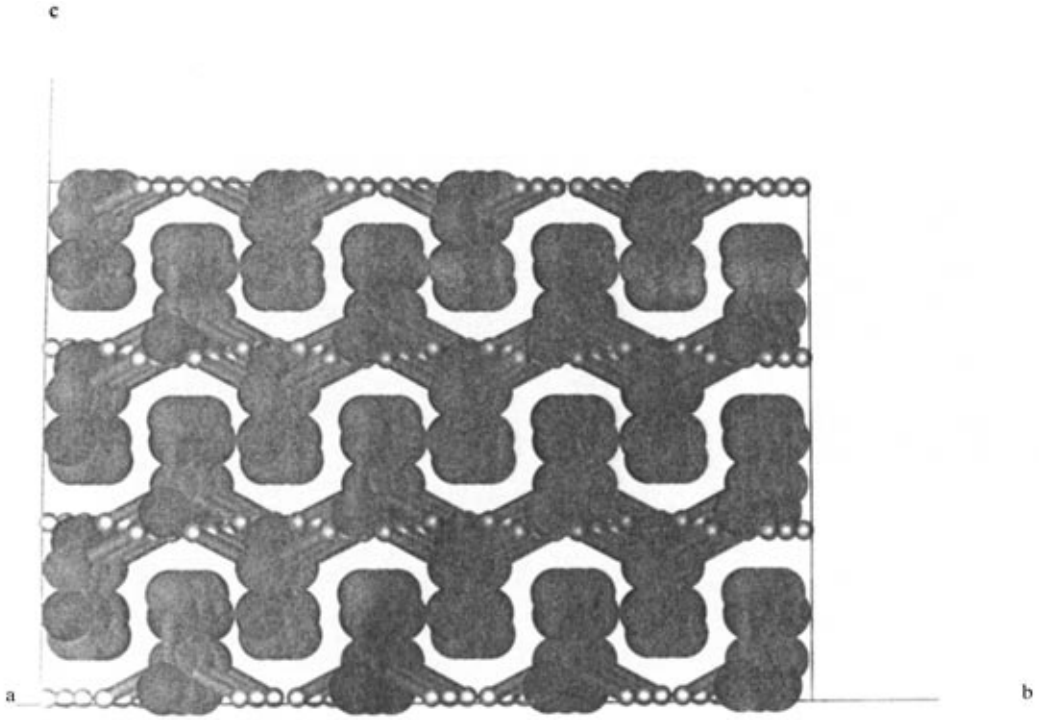

Fig. 3. Crystal structure of NH_4NO_3 (IV) viewed slightly off-axis from the *a* axis; hydrogen bonds are shown in green. The structure consists of pleated hydrogen-bonded sheets along **a** and **b**, with an absence of hydrogen bonding along **c**.

will become faster (Lewis, 1974*a*,*b*). High-index planes are molecularly rough and generally grow at a rate proportional to supersaturation or supercooling. If a saturated solution is initially cooled to an extent that produces moderate supersaturation and is then held at constant temperature, the crystals that form later will

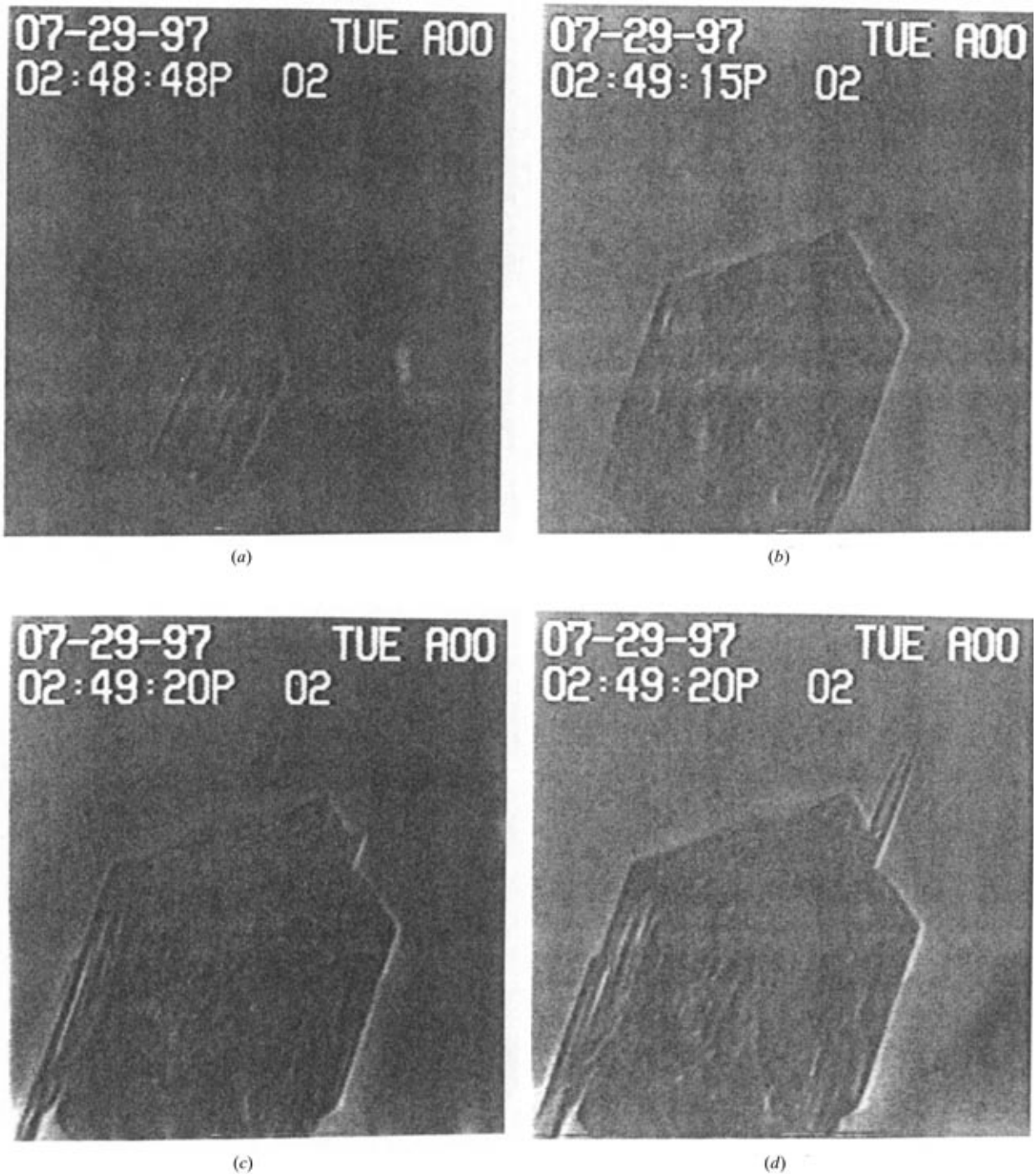

Fig. 4. (*a*) Interference photomicrograph of an $RbNO_3$ single crystal growing at 307 K. The long direction is [001]. The blue interference color in the area furthest from the crystal corresponds to the region of highest concentration. The vertical dimension of the photograph is 0.4 mm. (*b*) The same $RbNO_3$ single crystal as in (*a*) growing more rapidly. The concentration gradient is visible as a banded halo around the crystal. (*c*) The same $RbNO_3$ crystal as in (*a*) in accelerated growth 5 s later after rapid cooling to 302 K. The protrusion in the [001] direction reaches a region of high concentration (blue). (*d*) The same $RbNO_3$ crystal as in (*a*) 0.6 s later, showing a greatly exaggerated form due to continued growth of the [001] needle into a region of high concentration.

experience a lower degree of saturation. If the system is maintained at this temperature for an extended period, all the crystals will tend to approach the most energetically favorable morphology (this is akin to Ostwald ripening). In terms of growth conditions this evolution distinguishes 'early-growth' from 'late-growth' crystals. Our interpretation then of the morphological distortion observed in early-growth crystals is that, under conditions of moderate supersaturation, the critical supersaturation at which growth by two-dimensional nucleation is dominant has been exceeded for most of the crystal growth directions; however, there is one low-index growth direction for which the critical supersaturation is so high that it has not been met and which is thus still advancing only by screw dislocation growth. Therefore, advancement in this direction is retarded, relative to all others. As the supersaturation of the system falls below the critical values for the other faces, the morphology comes to be determined by screw dislocation growth for all low-index faces; this gives the late-growth morphology.

We have begun to look for structural characteristics that would allow the prediction of which direction will experience this distortion in a particular system. So far, we have found a clear rationale only in the case of NH_4NO_3 (IV). Here, the hydrogen bonding, which might be expected to be instrumental in stabilizing newly formed nuclei on growth surfaces, extends only in the *a* and *b* directions, forming hydrogen-bonded sheets as shown in Fig. 3. The absence of such attraction in the *c* direction may be the reason why {001} growth experiences early-growth relative retardation in this system.

Viewed in the light of our earlier studies of dendritic crystal growth, the present work suggests that the dendritic habit may be an extreme case of early growth morphology distortion. Among water-soluble ionic compounds, those forming dendrites from solution are to be found among compounds having a relatively high temperature coefficient of solubility. With such substances a high growth rate can be produced by appropriate cooling of their solutions; dendritic growth is produced by the most rapid cooling. Rapid cooling of a crystal/mother liquor system of such a material produces a steep concentration gradient in the solution adjacent to the crystal as solute begins to deposit on the crystal. In the sequence shown in Fig. 4 this concentration gradient is rendered visible with a double-beam interference microscope. It appears that the extreme morphological distortion characteristic of dendrites is caused by positive feedback between an initial morphology distortion brought on by high growth rate and the driving force of the concentration gradient surrounding the growing crystal. In the case of $RbNO_3$ (Fig. 4) the *c*-axis elongation corresponding to the early growth distortion seen in Fig. 1, column 4, causes the pyramidal termination of the crystal to intrude into the region of high concentration; the high concentration, in turn, causes a very large increase in the growth rate in that direction (Figs. 4*c* and 4*d*), which produces the needle crystal precursor to a dendrite. The connection between early growth morphology distortion and dendritic growth remains to be established for other systems.

The authors are grateful to The Petroleum Research Fund and the Simmons College Fund for Research for support of this work. We thank Drs Gillian Telfer, Robert Hammond and Kevin Roberts of Heriot-Watt University, Edinburgh, for instructive discussions. We also thank Drs Andrew Rohl and David Gay for making available the *MARVIN* software and for clarification of various points regarding its application.

References

Bats, J. W. (1978). *Acta Cryst.* B**34**, 1679–1681.
Bennema, P., Roberts, K. J. & Rohl, A. L. (1993). *Faraday Discuss.* **95**, 37–54.
Brice, J. C. (1973). *The Growth of Crystals from Liquids*, pp. 81–84. New York: Elsevier.
Burton, W. K., Cabrera, N. & Frank, F. C. (1951). *Philos. Trans. R. Soc. London Ser. A*, **243**, 299–358.
Chan, S.-K., Reimer, H.-H. & Kahlweit, M. (1976). *J. Cryst. Growth*, **32**, 303–315.
Choi, C. S., Mapes, J. E. & Prince, E. (1972). *Acta Cryst.* B**28**, 1357–1361.
Choi, C. S. & Prask, H. J. (1982). *Acta Cryst.* B**38**, 2324–2328.
Crystal Structure Design, AS (1997). *CrystalDesigner*. Version 6.0. PO Box 24 Blindern, N-0313 Oslo, Norway.
Dean, C., Hambley, T. W. & Snow, M. R. (1984). *Acta Cryst.* C**40**, 1512–1515.
Docherty, R., Clydesdale, G., Roberts, K. J. & Bennema, P. (1991). *J. Phys. D*, **24**, 89–99.
Dougherty, A., Kaplan, P. D. & Gollub, J. P. (1987). *Phys. Rev. Lett.* **58**, 1652–1655.
Dowty, E. & Richards, R. P. (1993). *SHAPE.* Version 4.2. 521 Hidden Valley Road, Kingsport, TN 37663, USA.
Ewald, P. (1921). *Ann. Phys.* **64**, 253–287.
Gay, D. H. & Rohl, A. L. (1995). *J. Chem. Soc. Faraday Trans.* **91**, 925–936.
Green, D. A., Harlow, R. L., Meenan, P., Robertson, D. C., Telfer, G. B., Roberts, K. J., Jackson, R. A. & Wilde, P. J. (1996). *Technologies Critical to a Changing World*, Vol. 5, pp. 692–697. 5th World Congress of Chemical Engineering. San Diego. New York: American Institute of Chemical Engineers (AIChE).
Hartman, P. & Strom, C. S. (1989). *J. Cryst. Growth* **97**, 502–512.
Johansson, G. B. & Lindqvist, O. (1977). *Acta Cryst.* B**33**, 2918–2919.
Karasawa, N. & Goddard III, W. A. (1989). *J. Phys. Chem.* **93**, 7320–7327.
Kuroda, T., Irisawa, T. & Ookawa, A. (1987). *Morphology of Crystals*, edited by I. Sunagawa, Part B, pp. 591–612. Boston: D. Reidel.
Lewis, B. (1974*a*). *J. Cryst. Growth*, **21**, 29–39.
Lewis, B. (1974*b*). *J. Cryst. Growth*, **21**, 40–50.
Nimmo, J. K. & Lucas, B. W. (1973). *J. Phys. C*, **6**, 201–211.
Rohl, A. L. & Gay, D. H. (1996). *J. Cryst. Growth*, **166**, 84–90.

Roberts, K. J., Telfer, G. B., Jackson, R. A., Wilde, P. J. & Meenan, P. (1995). *J. Chem. Soc. Faraday Trans.* **91**, 4133–4138.

Soltzberg, L. J., Fappiano, S. A., Griffith, L. D., Hidek, L. E., Ofek, S. A. & Suarez, L. L. (1994). *Acta Cryst.* B**50**, 518–524.

Soltzberg, L. J., Fappiano, S. A., Hidek, L. E., O'Brien, M. J. & Suarez, L. L. (1992). *Acta Cryst.* A**48**, 457–461.

Sunagawa, I. (1981). *Bull. Mineral.* **104**, 81–87.

Sunagawa, I. (1987). Editor. *Morphology of Crystals*, Part B, pp. 509–575. Boston: D. Reidel.

Telfer, G. B., Wilde, P. J., Jackson, R. A., Meenan, P. & Roberts, K. J. (1996). *Philos. Mag. B*, **73**, 147–152.

Wavefunction, Inc. (1997). *MacSpartan Plus*. Version 1.0. 18401 Von Karman Avenue, Irvine, CA 92612, USA.